Applications of Kirchhoff Least-Squares Migration: Towards Reservoir Imaging*

Francesco Perrone[1], Graham Roberts[1], Lorenzo Casasanta[1], Andrew Ratcliffe[1], Arash Jafargandomi[1], and Karen Purcell[1]

Search and Discovery Article #42183 (2018)**
Posted February 26, 2018

*Adapted from extended abstract based on oral presentation given at AAPG International Conference and Exhibition, London, England, October 15-18, 2017

[1]CGG, Crawley, United Kingdom (francesco.perrone@cgg.com)

Abstract

Seismic migration maps the acquired energy of the primary reflections into a structural image of the subsurface. In this process, the primary reflections are modeled as linear functions of the subsurface reflectivity. The mathematically rigorous procedure to reconstruct an image of such reflectivity is to apply the inverse of the modeling operator to the recorded data. However, because of the high dimensionality of the problem, this approach has historically been too computationally expensive for production-sized scenarios. Instead, a more practical imaging method has been preferred, the well-known migration operation, which consists of applying the adjoint of this forward operator to the recorded data. The adjoint here is not the inverse operator and, as a consequence, the migrated image is only an approximation of the Earth's true reflectivity. Specifically, in regions with more complex geological structure and complex wave propagation, the image can suffer from uneven subsurface illumination and artifacts caused by the deviation of the adjoint from the true inverse operator. A least-squares migration process approximates the application of the inverse operator and helps compensate these imaging issues. Using datasets from offshore Gabon and the Central North Sea, a practical workflow using non-iterative Kirchhoff least-squares migration demonstrates improved amplitude behavior, reduced image artifacts and image illumination compensation, as well as less noisy and better-focused AVO attribute sections. The Central North Sea data example also shows that adding seismic wave attenuation into the least-squares workflow generates a stable uplift in image resolution, in addition to the other benefits. Compared to the standard migration process, such improvements provide seismic amplitudes and images better suited for reservoir imaging.

Introduction

In an ideal world, seismic depth migration will create an image that represents the subsurface geological structure where reflection events recorded at the surface are re-positioned to their true location in the subsurface. In the real world, however, such a process is commonly contaminated with artifacts. In their review of the subject, Huang et al. (2014) highlight the detrimental effect on the image of: (i) under-sampled and irregular acquisition geometry; (ii) weak amplitudes resulting from geometrical spreading, attenuation and defocusing; (iii) areas of poor resolution resulting from limited recording aperture, and (iv) ringing artifacts caused by the finite bandwidth of the source wavelet. A good data pre-processing sequence can handle some of these issues. However, even if we assume that the velocity model is sufficiently

accurate, the basic problem remains: the migration operator is not the inverse of the forward single-scattering modeling operator but is its adjoint. A formal inversion procedure based on the least squares fit of the data aims to remove the migration artifacts and improve the amplitudes of the imaged reflectors – this is known as least-squares migration (Nemeth et al., 1999). Computation of the direct inverse for typical real-world applications is not currently tractable due to the extremely large dimensionality of the problem. Hence, the migration inverse problem is more commonly solved using an iterative, gradient-based, approach. Unfortunately, the iterative nature of this method makes it an expensive process involving multiple applications of costly migration and de-migration operators. However, the linear nature of this imaging problem means that some efficiency in the solution of the least-squares normal equations can be obtained by directly computing the Hessian matrix using point-spread-functions (Fletcher et al., 2015), or indirectly via non-stationary matching filters (Guitton, 2004). With these methods, the computational cost reduces to approximately a single iteration of an iterative scheme.

In recent years there has been increased interest in the field of least-squares migration due to examples showing an uplift on both synthetic and real data (Dong et al., 2012; Zhang et al., 2013; Fletcher et al., 2015; Valenciano et al., 2015; Duprat and Baina, 2016; Khalil et al., 2016; Wang et al., 2016; Bai et al., 2017; Casasanta et al., 2017; Huang et al., 2017; Wu et al., 2017). The least-squares migration process can be applied to any migration algorithm when the forward modeling and adjoint migration operators are available. In this paper, we apply it to a common-offset Kirchhoff migration. This migration scheme is still the workhorse imaging algorithm in many parts of the world, especially in the Europe, Africa and Middle East regions, due to its ability to generate high-frequency, high-resolution images with amplitude behavior consistent with Zoeppritz equations. In this paper we start by reviewing the theory behind least-squares migration, including seismic attenuation in the process, and discuss the practical workflow involved in implementing a Kirchhoff non-iterative (single-iteration), least-squares migration. We then demonstrate this workflow on two real data examples, one from offshore Gabon, without including attenuation, and the other from the Central North Sea where attenuation is part of the process. Finally, we draw some conclusions in our efforts towards improved reservoir imaging.

Least-Squares Migration Theory

We now recap the basic theory of least-squares migration, with specific reference to the Kirchhoff migration algorithm, although these general concepts are applicable to other migration schemes. We start with the acoustic setting, where seismic wave attenuation is ignored or assumed to be dealt with externally, and then move to the visco-acoustic modeling case, which includes seismic absorption as described by the quality factor (conventionally denoted as Q) of the medium.

Kirchhoff forward modeling (or de-migration) can be written as a linear operator:

$$d = Lr. \qquad (1)$$

In Equation (1) d is the acquired seismic data, L is the acoustic Kirchhoff modeling operator and r is the subsurface reflectivity. Solving the inverse problem, $r = L^{-1}d$, gives the desired subsurface reflectivity but, as mentioned before, computation of this direct inverse is not feasible

with real world seismic acquisition. The common alternative (Claerbout, 1992) is to apply the adjoint, L^H, of the forward operator, L, to the acquired data:

$$m = L^H d, \tag{2}$$

where m is the Kirchhoff migrated image. This image suffers from artifacts and illumination issues because the adjoint operator, not the inverse, is used. To mitigate these effects through the minimization of a least-squares cost function, $f(r) = \| d - Lr \|^2$, Nemeth et al. (1999) developed a formulation that matches modeled (de-migrated) data with observed data to update the migrated image. Solution of the least-squares normal equations gives the least-squares estimate of the subsurface reflectivity, r_{LS}:

$$r_{LS} = \left(L^H L\right)^{-1} L^H d, \tag{3}$$

where $L^H L$ is generally referred to as the Hessian operator. Equation (3) can be solved iteratively, for example, by using steepest descent or conjugate gradient methods.

The effects of an anelastic earth give rise to the absorption of seismic waves in the form of amplitude attenuation and phase distortion. Conventional acoustic migration assumes these (Q) effects are handled either pre- or post-migration. But standard migration can, in fact, be altered to directly compensate for these effects (Xie et al., 2009), by applying an amplitude boost and opposite phase distortion. Including Q in least-squares migration takes a different route to achieve the same goal, as we will now see. We start by modifying the modeling in Equation (1) to be

$$d = L_Q r, \tag{4}$$

where L_Q now represents the visco-acoustic Kirchhoff modeling operator (Wu et al., 2017). Again, we formulate the least-squares cost function, $f(r) = \| d - L_Q r \|^2$, and solve the normal equations to give a new version of Equation (3) that contains Q-compensation:

$$r_{LS} = \left(L_Q^H L_Q\right)^{-1} L_Q^H d. \tag{5}$$

Not too surprisingly, the functional form of Equation (5) is the same as that of Equation (3), with the only difference being the Kirchhoff modeling operator and its adjoint are now visco-acoustic and not just acoustic (for details, see Wu et al., 2017). Within this new operator, the absorption can be modeled by a so-called dissipation function, D:

$$D(x_s, y, x_r, \omega) = \exp\left[-\frac{\omega T^*}{2}\right] \exp\left[\left(\frac{i\omega}{\pi}\right) T^* \ln\left(\frac{\omega}{\omega_0}\right)\right], \tag{6}$$

where x_s and x_r are the shot and receiver coordinates, y is a generic point in the subsurface, ω is the temporal frequency, ω_0 the Q reference frequency and $T^*=T^*(x_s, y, x_r)$ is the dissipation time (which is a function of velocity and Q). We can see that the functional form of Equation (6) contains an imaginary exponential term to model the frequency-dependent phase distortion and a negative real exponential term to model amplitude attenuation, namely that the absorption effects mimic the same amplitude attenuation and phase distortion as the real earth. Once again Equation (5) can be solved iteratively by, for example, using steepest-descent or conjugate-gradient methods.

Non-Iterative (Single-Iteration) Least-Squares Migration Workflow

The multiple passes of migration and de-migration involved in the iterative solution of Equations (3) or (5) are computationally expensive. So we are right to ask the question: can we design a more cost-effective method? We start by substituting Equation (2) into Equation (3) to give:

$$r_{LS} = \left(L^H L\right)^{-1} m. \qquad (7)$$

This equation says that the least-squares estimate of the reflectivity is an inverse Hessian, (LHL)-1, filtered version of the migrated image. Consequently, the application of an estimate of the inverse Hessian matrix to the migration should reduce the artifacts in this image. Guitton (2004) proposed that this could be done with non-stationary matching filters following a de-migration / re-migration process. In particular, we perform:

a) An initial migration, m_0: $m_0 = L^H d$
b) A de-migration, d_0, of the data in a): $d_0 = L\, m_0$
c) A subsequent re-migration, m_1, of the data in b): $m_1 = L^H d_0 = (L^H L)\, m_0$
d) Design matching filters to match c) to a): $m_0 = (L^H L)^{-1}\, m_1$
e) Apply the matching filters from d) to the data in a): $r_{LS} = (L^H L)^{-1}\, m_0$

As can be seen in c), Guitton (2004) observed that the effect on the migrated image of the cascade a) → c) is precisely the Hessian, whose inverse we wish to estimate through matching filters in d), and final application to a). This approach was developed further by both Khalil et al. (2016) and Wang et al. (2016), particularly by the use of curvelet domain filters for improved stability and structural consistency in the matching process (Wang et al., 2016). The cost of this non-iterative least-squares migration process, with its de-migration / re-migration mechanics, is similar to that of a single iteration of an iterative scheme, making it more cost-effective than the traditional iterative approach.

This approach also works if Q is included in the workflow with the Kirchhoff modeling operator and its adjoint being visco-acoustic: $m_0=L_Q^H d$ and $m_1 = (L_Q^H L_Q)\, m_0$. It is interesting to note that at no stage in this least-squares migration process do we apply a formal Q-compensating migration, as would be done in standard migration to remove the effects of Q. Instead, each migration / de-migration step is now an attenuating step (with associated phase behavior) and the matching filter captures this, such that when applied to the initial migration we obtain a Q-compensated image (Wu et al., 2017).

Since visco-acoustic Kirchhoff forward and adjoint operators are, in general, more computationally demanding than their acoustic versions, least-squares migration with Q is a more expensive process. One can design more cost-effective approaches, involving the application of only one visco-acoustic operation and conventional acoustic migrations / de-migrations (Y. Xie and P. Wang, personal communication, 2016), by stepping away from the formal least-squares migration framework of Equation (5) to form:

$$r_{LS} = \left(L^H L_Q\right)^{-1} L^H d, \tag{8}$$

or

$$r_{LS} = \left(L_Q^* L\right)^{-1} L^H d, \tag{9}$$

where the new symbol, L_Q^*, denotes a migration operator with the same amplitude and phase behavior of the visco-acoustic modeling (de-migration) operator, as opposed to being the formal adjoint.

Offshore Gabon Real Data Example

A very large, 25,000 km^2, 3D marine seismic survey was acquired over the deep-water part of the South Gabon Basin in 2014 and 2015 using a variable-depth towed-streamer configuration (Soubaras and Dowle, 2010) for low-noise, broad-bandwidth data. Kirchhoff depth migration gives detailed structural images but the presence of salt bodies result in crosscutting swing artifacts and uneven illumination in some locations, as shown in the constant offset (565 m) conventional migrated section in Figure 1a and highlighted by the arrows. We have applied the non-iterative, single-iteration, (acoustic) Kirchhoff least-squares migration to a portion of this dataset and Figure 1b shows that the close-to-vertical migration swing artifacts are reduced. We also see reduced speckled noise, improved event coherency and a better-balanced illumination in the overall image, highlighted by the arrows in the images. For the sake of a fair comparison, it is important to note that the seismic data from which these two Kirchhoff images are generated has the same pre-processing sequence applied, which includes all of the elements (de-ghosting, spectral balancing, regularization and interpolation) that are designed to improve the quality of the standard Kirchhoff image, as well as the usual de-multiple and de-noise pre-processing steps.

Stack comparison of this area is shown in Figure 2. The stack itself is a good attenuator of some of the standard migration artifacts, such as the swings and the speckled noise, but clearly, it cannot perform illumination compensation and may not attenuate all of the artifacts. The comparison of Figure 2a to 2b highlights these aspects, with the least-squares migration providing a better image. The ovals highlight the areas where illumination is better balanced and swing artifacts are attenuated; the arrows point to improved continuity of weaker events.

The act of stacking over offset disregards the pre-stack amplitude versus offset (AVO) information; hence, one of the key benefits of the least-squares migration process is to reduce the conventional migration artifacts on the pre-stack data. This should lead to better AVO products after the least-squares migration. Figure 3 shows the AVO gradient sections of the data from Figure 1 and Figure 2 and the arrows point to where

this behavior is apparent. We see reduced noise (speckle and swing) on the AVO gradient derived from the least-squares process compared to the standard migration, as well as areas where the AVO gradient clearly changes because of the improved illumination. Unfortunately, there is no well data available in this area to allow us to make a formal comparison of well and seismic reflectivity or AVO. Figure 4 shows the AVO intercept vs. gradient cross-plot obtained from standard and least squares migration for the portion of Figure 1 and Figure 2 shown in the insets. In general, we see a tighter correlation in the cross-plots derived from the least-squares migration data due to reduced migration artifacts/noise in the underlying seismic data. The denoised and more coherent AVO gradient allows us to identify a clearer trend in the cross-plot after least-squares migration. Finally, for this data set, we perform an AVO inversion to derive P-impedance and Vp/Vs sections – these are displayed in Figure 5a and 5b for the standard migration and Figure 5c and 5d for the single-iteration least-squares migration. Least squares Kirchhoff inversion leads to more coherent estimates of the P-impedance and Vp/Vs sections; the insets in Figures 5b and 5d show the tightening of the P- and S-impedance cross-plot in the least-squares result. The graphs at the top of the panels in Figure 5 display the correlation coefficient between the real data and data synthesized from the AVO inversion result: a value closer to unity indicates that the data synthesized from the least squares sections are a better match to the real data.

Central North Sea Real Data Example

We demonstrate the non-iterative, single-iteration, visco-acoustic, Kirchhoff least-squares migration on a 3D marine seismic survey acquired in Quad 22 of the UKCS Central North Sea. This data was part of a much larger data set consisting of multiple conventional and variable-depth, narrow-azimuth towed-streamer acquisitions (Hollingworth et al., 2015). Our interest is to see if, in addition to the other benefits, visco-acoustic least squares migration can help stabilize the uplift of Q in the imaging process. Figure 6 shows a zoom of a common-offset (480 m) depth migrated section that contains geology typical of the region, namely mildly dipping horizons (the upper Cretaceous Chalk package) that overlie the Base Cretaceous Unconformity (BCU). To evaluate the impact of the visco-acoustic least-squares migration process, we compare it with a Q-compensating migration. The value of Q used in both Q-compensating migration and single-iteration Q least-squares inversion is constant and equal to 150. In generating the Q-compensating migration, a processing choice must be made as to what dB limit we threshold the Q boost. This is necessary in all Q-compensating processes, not just migration, to avoid boosting too much noise at the higher frequencies. Figure 6a shows the standard Q-compensating migration with a Q-limit of +15 dB; a +20 dB image was also generated and does lead to a slightly higher resolution being obtained, but boosts too much noise at the higher frequencies. Figure 6b shows the result from visco-acoustic least-squares migration where a clear uplift is observed in the quality of the image, especially in the chalk package that is seen to suffer from strong migration swing noise, in terms of de-noise, improved event coherency, more balanced illumination and a stable increase in resolution (as indicated by the arrows). This is backed up by comparison of the amplitude spectra in Figure 7 where we include both the +15 dB and +20 dB Q-compensated results. The visco-acoustic least-squares migration gives us the best of both worlds in terms of squeezing the most out of the resolution, without boosting the noise.

Figure 8 shows the improvement over the Q-compensating migration on the stack and offset gathers. By accounting for Q in the least-squares inversion, we improve illumination across the section and in particular, below the chalk package, as highlighted by the ovals; moreover, in the offset gathers, the arrows point to areas where we observe improved resolution and illumination as function of offset. As before, we note that the same data with the same data pre-processing is used in the imaging, and that this processing was designed to improve the quality of the standard Kirchhoff image.

Conclusions

Despite its limitations in relation to multi-pathing and ray-tracing in very complex geological settings, Kirchhoff migration still represents the main imaging algorithm in many areas of the world, and in particular the Europe, Africa and Middle-East regions. Kirchhoff migration produces, in a cost-effective way, high-frequency pre-stack depth images with reliable amplitude behavior as function of offset or incidence angle, and thus is particularly suitable for AVO/AVA analysis and reservoir imaging. The formulation of the imaging problem as a linear problem allows us to implement an approximate inversion of the data in terms of reflectivity in a single step, i.e. without need to iterate to minimize the data matching objective function. The non-iterative approach is based on a non-stationary image deconvolution in the curvelet domain. Real data examples from offshore West Africa and the Central North Sea prove that the method is stable, robust and cost-effective for production-size datasets. The inverted images show improved illumination, and better signal-to-noise ratio and the standard migration artifacts introduced by Kirchhoff migration in the areas with more complex geology and in the presence of salt bodies are effectively attenuated. The uplift in the pre-stack images is important for the estimation of AVO attributes, in particular the AVO gradient, which is notoriously sensitive to noise. The single-iteration least-squares migration approach can be extended to include attenuation. Our examples show that the inclusion of Q in the least-square migration procedure allows us to automatically control the trade-off between signal amplification and noise attenuation.

Acknowledgements

We thank CGG for permission to publish this work, CGG's Multi-Client & New Ventures business line for permission to show the real data examples and the numerous R&D and production colleagues within CGG who have helped with the least-squares algorithm and real data examples.

References Cited

Bai B., Y. Song, and Y. Lui, 2017, From full waveform inversion to Kirchhoff least-squares migration – correcting the effects of mass-transport complexes for better reservoir imaging: 79th EAGE Conference and Exhibition, EAGE, Extended Abstracts We A3 06.

Casasanta, L., G. Roberts, F. Perrone, A. Ratcliffe, G. Poole, Y. Wang, and Y. Xie, 2017, Practical benefits of Kirchhoff least-squares migration deconvolution: 79th EAGE Conference and Exhibition, EAGE, Extended Abstracts Tu B3 06.

Claerbout, J., 1992, Earth sounding analysis: processing versus inversion: Blackwell Scientific Publications.

Dong, S., J. Cai, M. Guo, S. Suh, Z. Zhang, B. Wang, and Z. Li, 2012, Least-squares reverse time migration: towards true amplitude imaging and improving the resolution: 82nd Annual International Meeting, SEG, Expanded Abstracts, 1-5.

Duprat, V., and R. Baina, 2016, An efficient least-squares reverse-time migration using true-amplitude imaging condition as an optimal preconditioner: 78th EAGE Conference and Exhibition, EAGE, Extended Abstracts, We SRS2 12.

Fletcher, R.P., D. Nichols, R.M. Bloor, and R.T. Coates, 2015, Least-squares migration: data domain versus image domain: 77th EAGE Conference and Exhibition, EAGE, Extended Abstracts, We N106 06.

Guitton, A., 2004, Amplitude and kinematic corrections of migrated images for non-unitary imaging operators: Geophysics, v. 69, p. 1017–1024.

Hollingworth, S., O. Pape, C. Purcell, E. Kaszycka, T. Baker, J. Cowley, G. Duval, L. Twigger, 2015, Setting new standards for regional understanding - mega-scale broadband PSDM in the North Sea: First Break, v. 33/9, p. 75–79.

Huang S., M. Wang, B. Bai, and P. Wang, 2017, Improving Subsalt Imaging with Least-Squares RTM - A case study at Kaskida field, Gulf of Mexico: 79th EAGE Conference and Exhibition, EAGE, Extended Abstracts Tu B3 07.

Huang, Y., G. Dutta, W. Dai, X. Wang , G.T. Schuster, and J. Yu, 2014, Making the most out of least-squares migration: The Leading Edge, v. 33/9, p. 954-960.

Khalil, A., H. Hoeber, G. Roberts, and F. Perrone, 2016, An alternative to least-squares imaging using data-domain matching filters: 86th Annual International Meeting, SEG, Expanded Abstracts, 4188-4192.

Nemeth, T., C. Wu, and G.T. Schuster, 1999, Least-squares migration of incomplete reflection data: Geophysics, v. 64, p. 208-221.

Soubaras, R., and R. Dowle, 2010, Variable-depth streamer – a broadband marine solution: First Break, v. 28/12, p. 89–96.

Valenciano, A., S. Lu, N. Chemingui, and J.Yang, 2015, High-resolution Imaging by Wave-Equation Reflectivity inversion: 77th EAGE Conference and Exhibition, EAGE, Extended Abstracts, We N103 15.

Wang, P., A. Gomes, Z. Zhang, and M. Wang, 2016, Least-squares RTM: Reality and possibilities for subsalt imaging: 86th Annual International Meeting, SEG, Expanded Abstracts, 4204-4209.

Wu X., Y. Wang, Y. Xie, J. Zhou, D. Lin, and L. Casasanta, 2017, Least square Q-Kirchhoff migration: implementation and application: 79th EAGE Conference and Exhibition, EAGE, Extended Abstracts Tu A1 08.

Xie, Y., S.K. Xin, J. Sun, C. Notfors, A.K. Biswal, and M.K. Balasubramaniam, 2009, 3D prestack depth migration with compensation for frequency dependent absorption and dispersion: 79th Annual International Meeting, SEG, Expanded Abstracts, 2919-2923.

Zhang, Y., L. Duan, and Y. Xie, 2013, A stable and practical implementation of least-squares reverse time migration: 83rd Annual International Meeting, SEG, Expanded Abstracts, 3716-3720.

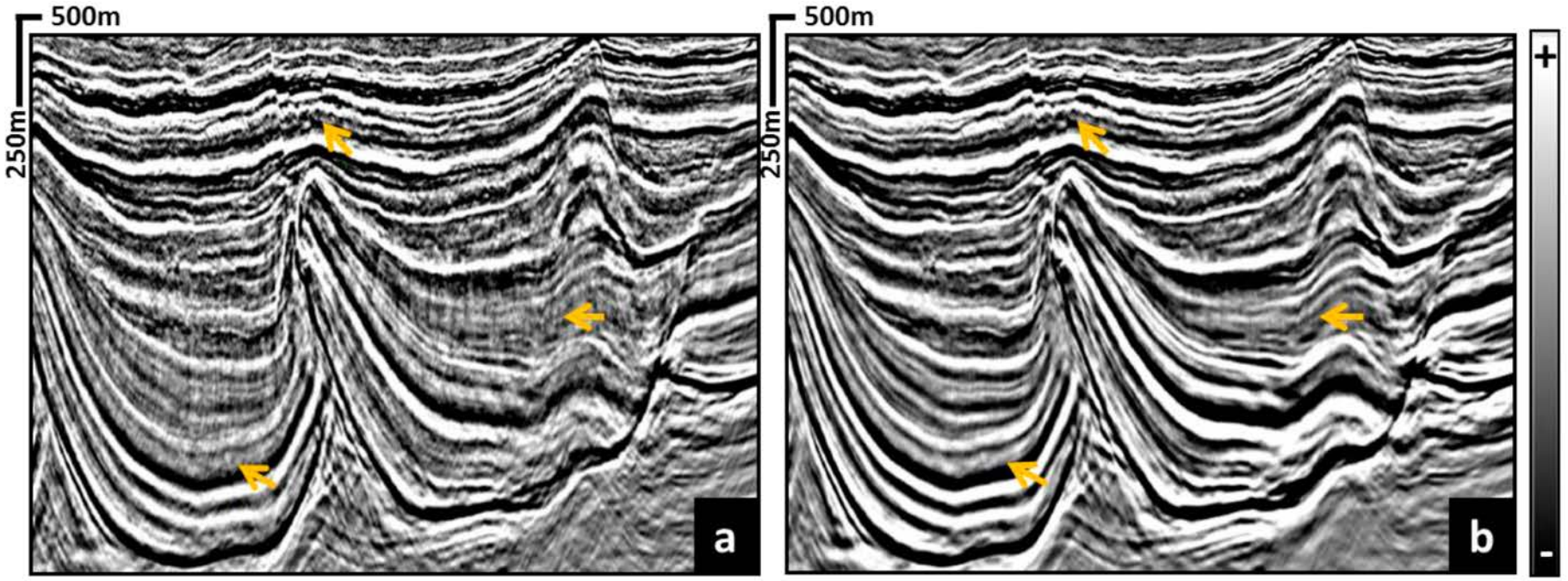

Figure 1. Single offset (565 m) comparison: (a) conventional migrated image, and (b) single-iteration least-squares migration result. The result in (b) shows better event continuity, illumination and noise attenuation.

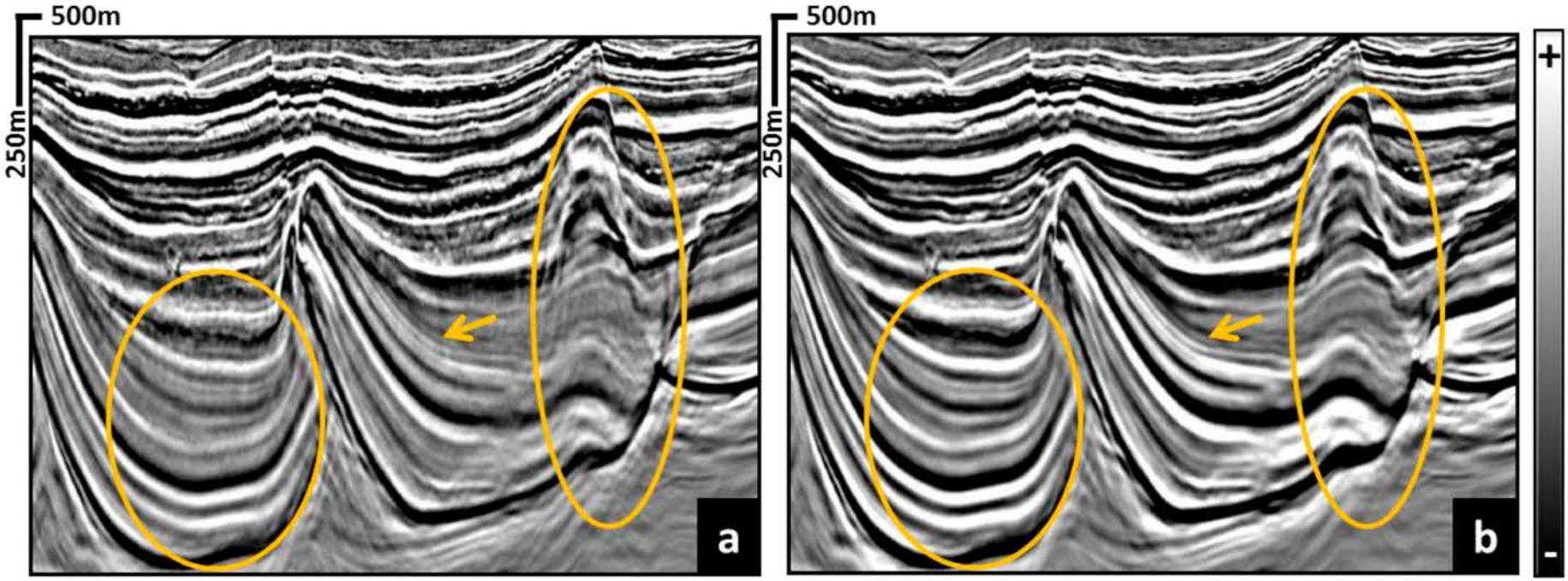

Figure 2. Stack comparison: (a) conventional migration, and (b) single-iteration least-squares migration. The least-squares result in (b) improves illumination and further attenuates migration swing artifacts.

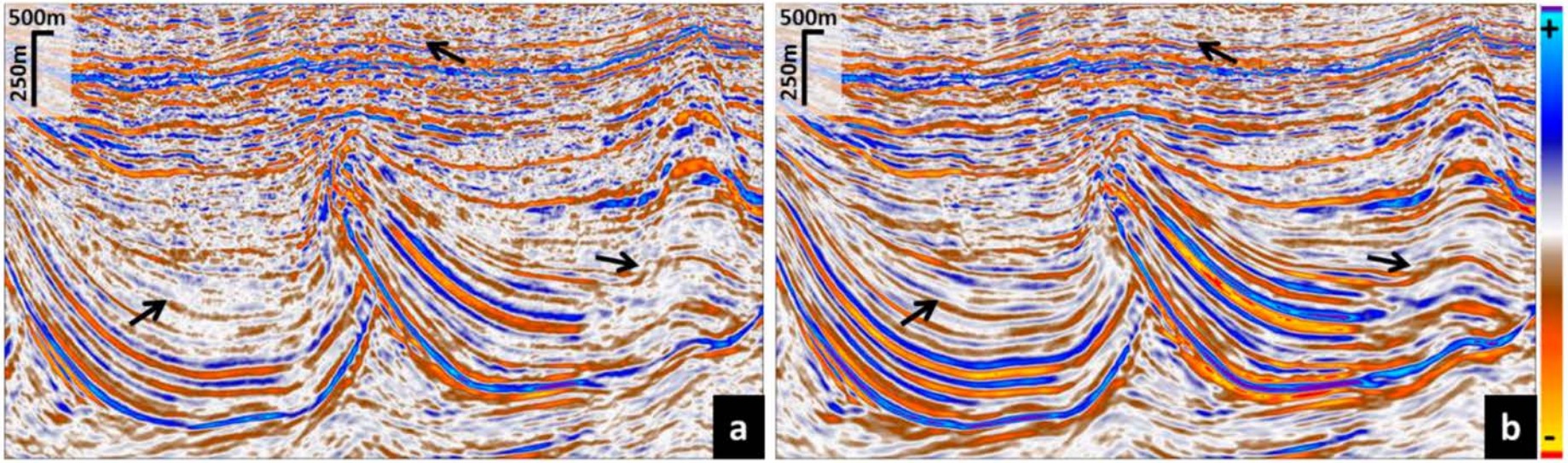

Figure 3. AVO gradient comparison: (a) conventional migration, and (b) single-iteration least-squares migration. The presence of noise and migration smiles contaminate the AVO gradient estimation in (a). Least-squares inversion improves illumination and signal-to-noise ratio thus stabilizing the AVO gradient.

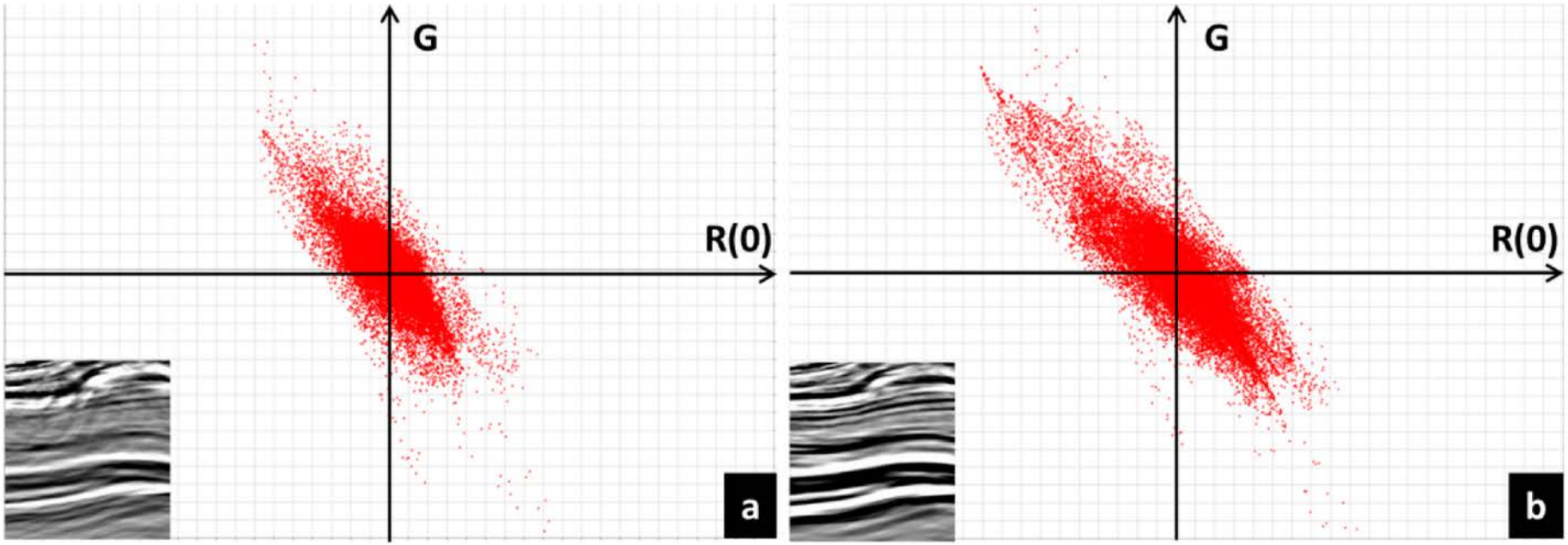

Figure 4. AVO cross-plot comparison of intercept (R0) against gradient (G) for the window of the same area from Figure 1 and Figure 2 shown in the insets: (a) cross-plot from the conventional migrated image, and (b) cross-plot from the single-iteration least-squares migration result. Notice the emergence of a clearer trend in the least-squares result cross-plot due to the enhanced coherency of the AVO gradient.

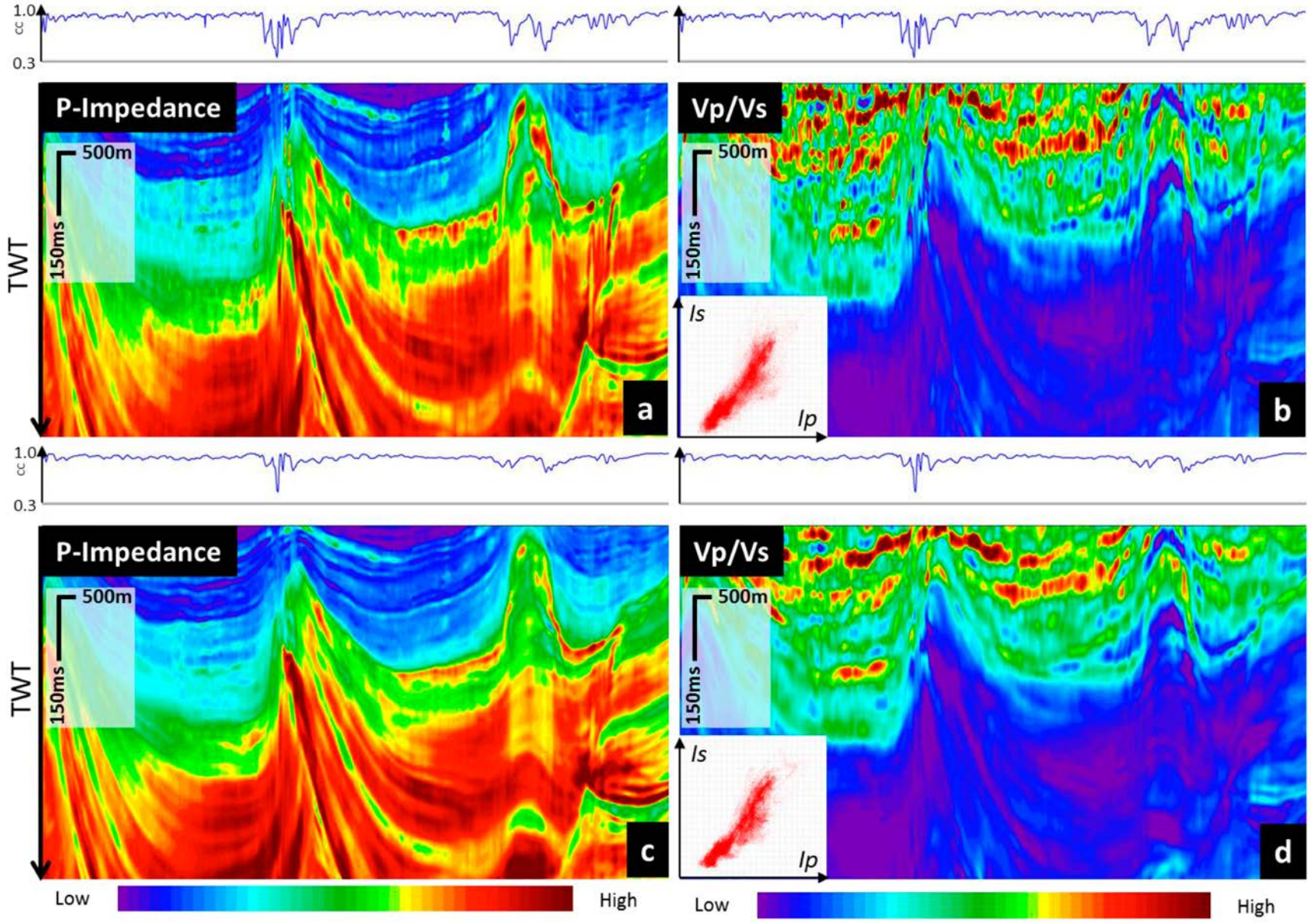

Figure 5. AVO inversion comparison for the same area from Figure 1 and Figure 2. (a) and (b) show the P-impedance and Vp/Vs estimated from conventional migration result. The inset in (b) shows the cross-plot of shear and compressional impedances. The graphs at the top of the Figures show the correlation between synthesized and real data. (c) and (d) show the same inversion results after single-iteration least-squares migration. Notice the improved continuity of the estimates, the tightening of the cross-plot and the higher correlation values between synthesized and real data, particularly in areas of complex imaging.

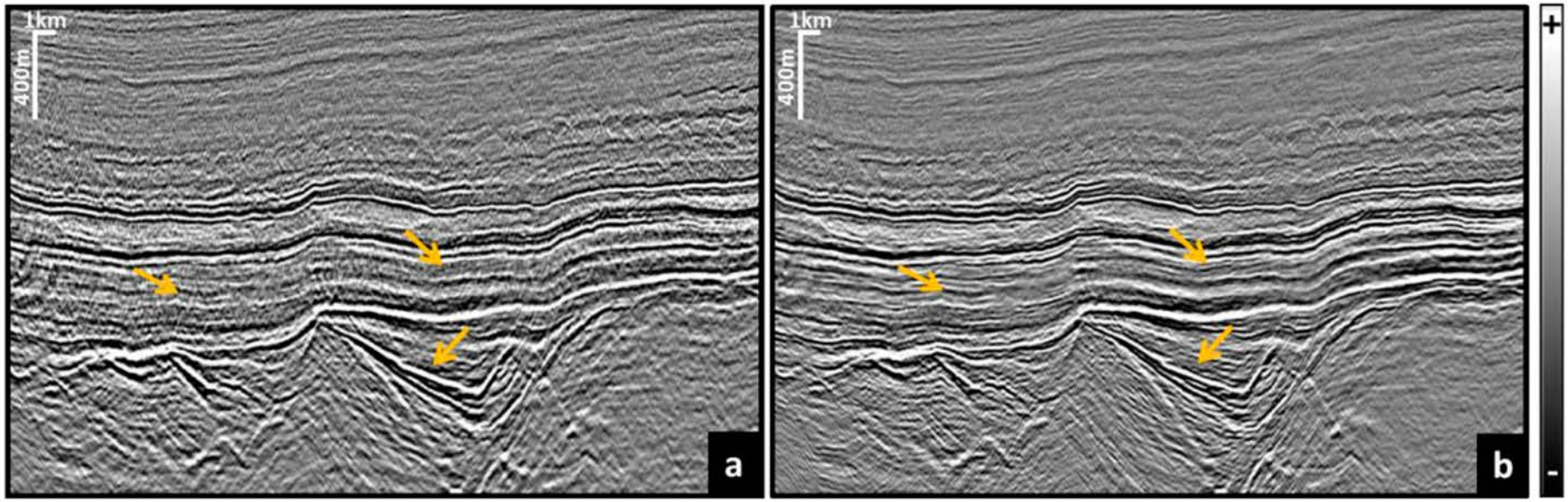

Figure 6. Single offset (480 m) comparison: (a) Q-compensating migration (+15 dB limit), and (b) single-iteration Q least-squares migration. Notice the improved resolution and control over noise in the areas highlighted by the arrows.

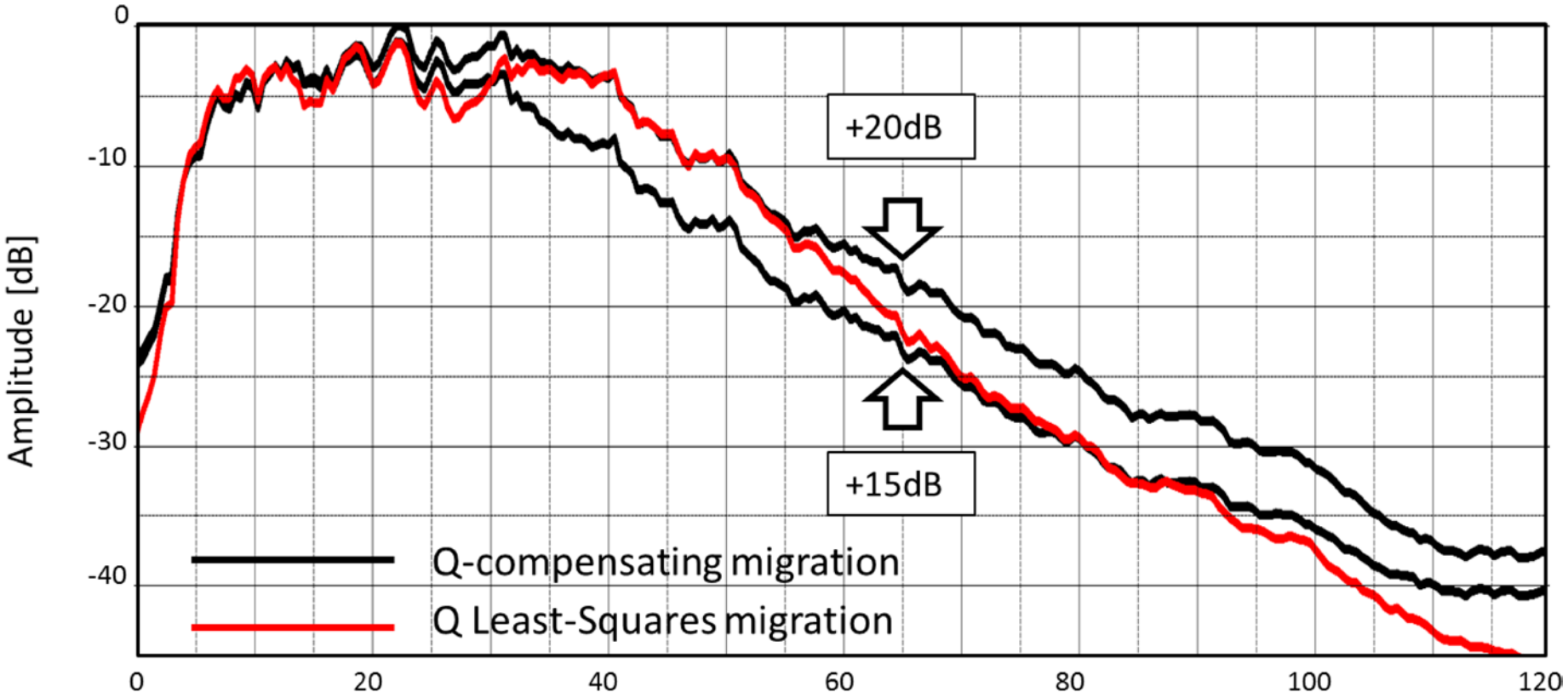

Figure 7. Comparison of the image spectra from two Q-compensating migrations (with different dB limits) and the single-iteration Q least-squares migration. Notice the automatic control in terms of signal amplification and noise attenuation in the least-squares inversion result.

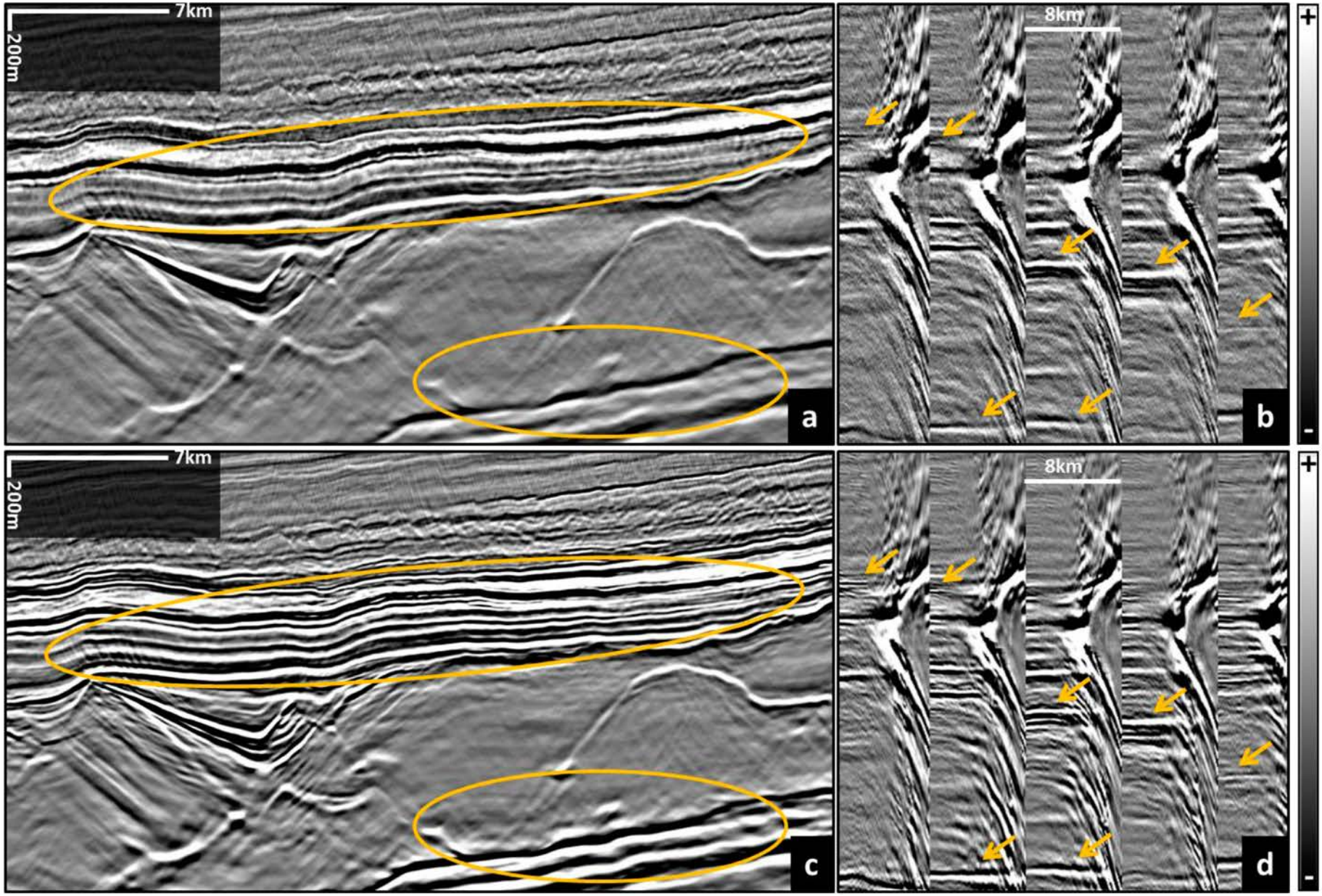

Figure 8. Stack and gathers comparison: (a) Q-compensating migration stack (+15 dB limit), and (c) single-iteration Q least-squares migration stack. Notice the improved illumination and increased resolution across the section. In comparison to the gathers from the migration result (b), those from the single-iteration Q least-squares migration show enhanced illumination and resolution as function of offset (d).